Bilayer Nanocomposite Molecular Coatings from Elastomeric/Rigid Polymers: Fabrication, Morphology, and Micromechanical Properties

Igor Luzinov[$, &], Daungrut Julthongpiput[$], Paul D. Bloom[#], Valerie V. Sheares[#], Vladimir V. Tsukruk[$*]

[$]Department of Materials Science & Engineering, Iowa State University, Ames, Iowa 50011, USA
[#]Department of Chemistry, Iowa State University, Ames, Iowa 50011, USA
[&]School of Textiles, Fiber and Polymer Science, Clemson University, Clemson, South Carolina 29634, USA

SUMMARY: We fabricated bilayered nanocomposite coatings composed of a hard polymer layer placed on top of an elastomeric layer. The primary layer of poly[styrene-*b*-(ethylene-*co*-butylene)-*b*-styrene] (SEBS) was attached to the surface by grafting to a chemically reactive silicon surface functionalized with epoxy-terminated SAM. The SEBS layer served as the compliant interlayer in the bilayered polymer coating. The topmost hard layer was a high performance polymer made of epoxy resin (EP) and an amino functionalized poly(paraphenylene) (PPP). We built the bilayered structure by spincoating the EP/PPP mixture on top of the grafted SEBS layer. The solidification of the topmost layer was initiated at low temperatures (40 – 50 °C) to avoid dewetting. The curing of the film was finished at 110 °C (15 hours) and the EP/PPP layer was strongly attached to the SEBS layer. It was found that the EP/PPP layer did not penetrate inside the elastic primary layer during the solidification. The elastic response of the hard polymer layer was affected significantly by the underlying elastomeric layer. The SEBS layer served as a compliant interlayer capable of dissipating the interfacial stresses originating from dissimilarities in the physical properties between the polymer coating and the inorganic substrate.

Introduction

The fabrication of stable and homogeneous thin polymeric films is important in many practical coatings such as lubricants, adhesives, and protective coatings [1-5]. High performance polymer coatings possessing excellent mechanical and environmental stability can be deposited on the inorganic surface. However, there are two major

* To whom correspondence should be addressed: vladimir@iastate.edu

 CCC 1022-1360/00/$ 17.50+.50/0

problems in the fabrication and utilization of these thin films. First of all, wettability controls the stability and morphology of the films during preparation and use. A number of factors effect the dewetting of polymer films. Among them are thickness, polymer-surface interaction, viscosity, temperature, and surface tension [6]. It isnecessary to note that spincoating can produce metastable polymer films even on an nonwettable surface. Nonetheless, the thin film will dewett the substrate if heated above the glass transition temperature [2, 4-7].

Another challenge in the design of high performance polymer coatings is the enormous dissimilarity in physical properties between the inorganic substrate and the polymer deposited [8]. For instance, typical values of Young's modulus for polymers are 10 – 1000 times lower than the values for the inorganic material. In addition, the thermal expansion coefficient for inorganic materials is 5 – 10 times lower. These differences can create large stresses at the interface and lead to its rupture, delamination, or buckling [9]. Furthermore, thin coatings often develop residual compressive stresses during the deposition process [9, 10]. Deposition of an ultrathin elastomeric interlayer between a high performance polymer film and an inorganic surface could alleviate this interfacial problem. For example, the interlayer can reduce the deformations in the film resulting from the difference in the thermal expansion coefficients, or reduce the stresses developed within the film if mechanical force is applied to the interface. Consequently, in the present work, we focus on the preparation of thin bilayer polymer films consisting of a hard polymer layer separated from the inorganic substrate by a compliant elastomeric layer.

The primary elastomeric layer was formed from the thermoplastic elastomer, poly[styrene-*b*-(ethylene-*co*-butylene)-*b*-styrene] (SEBS) functionalized with 2% of maleic anhydride (MA) randomly imbedded into the hydrocarbon chains. To avoid dewetting and to stabilize the elastomeric ultrathin film, functionalized SEBS was grafted on a specially prepared, chemically functionalized silicon surface [11]. The epoxy-terminated self-assembled monolayer (SAM) deposited on a silicon wafer prior to block copolymer layer fabrication was used as an anchoring surface. Previously, it was shown that for these homogeneous and robust SAMs, terminal epoxy groups were mainly located at the monolayer surface [12, 13].

The topmost hard layer was a high performance polymer made of the epoxy resin (EP) and an amino functionalized poly(paraphenylene) (PPP) (Scheme 1). The polymer coating formed a cross-linked structure due to the reaction between epoxy groups of EP and amino groups of PPP. It is known that the use of cross-linkable polymer materials for film fabrication can prevent the film dewetting from occurring [14]. Additionally, the reaction between the functional (epoxy and amino) groups of the upper layer, and the MA groups of primary elastomeric layer may stabilize the morphology of the EP/PPP layer.

We believe that a combination of two distinct polymer layers in one nanocomposite coating can bring new opportunities for design of thin polymer coatings. The high performance top layer will face external physical or chemical impact. The underlying rubbery layer will reduce stresses and deformations occurring from the mismatch of physical properties between the inorganic substrate and the deposited polymer.

Experimental

The epoxysilane compound, (3-glycidoxypropyl)trimethoxysilane was purchased from Gelest Inc. ACS grade toluene and ethanol were obtained from Aldrich and were used as received. Highly polished single-crystal silicon wafers of {100} orientation (PureSilicon, Inc.) were used as substrates. The wafers were first cleaned in an ultrasonic bath for 30 minutes, placed in a hot piranha solution (3:1 concentrated sulfuric acid/ 30% hydrogen peroxide) for one hour, and then rinsed several times with high purity water (18 MΩ cm, Nanopure). After the rinsing, the substrates were dried under a stream of dry nitrogen, immediately taken into the nitrogen-filled glove box, and immersed in an epoxysilane solution (1 volume %) for 24 hours. After the deposition was completed, modified substrates were removed from solution, and rinsed several times with toluene and ethanol. All sample fabrication was conducted under cleanroom 100 conditions.

The chosen SEBS copolymer was Kraton 1901 (Shell) with a styrene and maleic anhydride content of 29 wt. % and 2 wt. %, respectively. The molecular weight measurements were carried out for the SEBS solution in THF using a Waters-GPC

equipped with Mini Dawn (Wyatt Technology) light scattering detector. GPC data showed $<M_n>$ = 41,000 g/mol, $<M_w/M_n>$ =1.16, and R_g = 6.3 nm, where R_g is the radius of gyration of SEBS macromolecules. The SEBS copolymer films were deposited on the epoxy-terminated SAM from melt. The MA groups of the rubbery block poly(ethylene-co-butylene) (PEB) were able to react with the epoxy groups of the monolayer [15], thus anchoring the rubber block to the surface.

The initial SEBS film was spin-coated from a toluene solution (1.5 wt. %) onto the epoxysilane modified silicon wafer. The initial thickness of the spin-coated film measured by ellipsometry was 60 ± 6 nm. The specimen was placed in a vacuum oven at 150 °C for 120 minutes to enable the MA groups to diffuse and graft to the epoxy-terminated substrate. In all experiments, the unbound polymer was removed by multiple washing with toluene including the washing in an ultrasonic bath. After nine washes, the thickness of the layer did not decrease with additional treatment in an ultrasonic bath.

The EP was Novolac resin D.E.N. 431™ provided by Dow Chemical. The amino functionalized PPP was prepared in a two step synthesis. First, poly(4'-fluoro-2,5-diphenylsulfone) (P1) was synthesized via Ni(0) catalyzed coupling of 2,5-dichloro-4'-fluorodiphenylsulfone [16]. Nucleophilic aromatic substitution of P1 with 4-aminophenol gave the amino functionalized PPP (Scheme 1). Gel permeation chromatography and ^{1}H-NMR results showed the substitution of 4-aminophenol to be nearly quantitative. The characterization results of poly(4'-fluoro-2,5-diphenylsulfone) and the amino functionalized PPP have been summarized in Table 1.

To estimate the bulk properties of EP/PPP material, EP was mixed and reacted with an equivalent amount of PP (EP/PPP = 0.9/1.0 (wt./wt.)) at 150 °C for 1 hour and 200 °C for 6 hours. The resulting crosslinked material has excellent solvent resistance to DMAc, *m*-cresol and THF, with no weight gain after a 24 hour immersion period in each solvent. Differential scanning calorimetry showed a glass transition temperature of 175 °C. Thermogravimetric analysis of the amino PPP cured epoxy had 5 and 10% weight loss values in air of 392 and 408 °C, respectively.

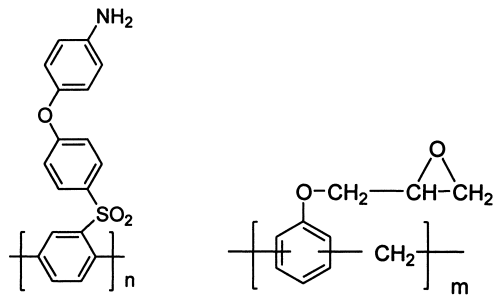

PPP **Novolac Epoxy**

Scheme 1 The structure of oligomers used for the synthesis of the upper layer. n = 5 - 6; m = 3 - 4.

Table 1. GPC, NMR, DSC, and TGA Results for Poly(4'-fluoro-2,5-diphenylsulfone) (PI) and 4-aminophenol derivative (PPP)

Sample	M_n>, Theor.[a]	<M_n>[b]	PDI[b]	T_g (°C)[c]	N_2 (°C)[d]	5% air (°C)[d]	N_2 (°C)[d]	10% air (°C)[d]
P1	-	1160	1.43	144	443	437	484	476
PPP	1610	1610	1.34	167	434	437	485	486

[a]: theoretical <M_n> calculated for 100 % substitution of **P1** with 4-aminophenol.
[b]: data obtained by GPC. [c]: data obtained by DSC. [d]: data obtained by TGA.

The EP/PPP layers were deposited by spincoating of the EP/PPP mixture (0.9/1.0 (wt./wt.)) dissolved in THF. Different concentrations (0.15% - 0.7%) of EP/PPP solution were used to produce top layers with the thicknesses from 4 nm to 22 nm as was measured by ellipsometry. The specimens were cured in a vacuum oven at various temperatures (45 – 110 °C).

Film surfaces were examined by static contact angle (sessile droplet) measurements using a custom-designed optical microscope system. Droplets (1.5 - 2 μl) of Nanopure water were placed randomly over the surface. Contact angles were determined within 1 minute after the droplet deposition. All reported values were averaged over at least six measurements. The shape of the droplets was observed with a microscope equipped with a CCD camera, and the contact angle was measured on the monitor screen.

Ellipsometry was performed with a COMPEL automatic ellipsometer (InOmTech, Inc.). The angle of incidence used was 70°. The silicon oxide thickness was measured for each silicon wafer after the piranha solution treatment and before film deposition. The thickness of the silicon oxide layer was determined to be within 0.8 - 1.2 nm for different wafers. The indexes of refraction of the epoxysilane monolayer and silicon oxide were considered to be equal to the "bulk" values [13]. The refractive indexes for SEBS, EP, and PPP were estimated by additive molar contributions [17]. All reported thickness values were averaged over six measurements. Scanning probe microscopy (SPM) studies were performed in the tapping mode on a Dimension 3000 (Digital Instruments, Inc.) microscope according to the procedure described earlier [18, 19]. Silicon cantilevers had spring constants of about 50 N/m. Imaging was done with scan rates in the range 1 - 2 Hz.

Results and discussion

SEBS grafted layer: morphology and properties

The thickness and contact angle were measured for the SEBS film grafted to epoxysilane SAM. The thickness of the SEBS film measured by ellipsometry was approximately 8.5 nm. This is a monolayer, since the thickness is lower than the size of unperturbed SEBS macromolecule (12.3 nm). The water contact angle for the film was nearly 100°. The contact angle value indicated that the surface of the block copolymer films was completely occupied by poly(ethylene-*co*-butylene) chains of SEBS [20, 21].

The SPM topographical image of the SEBS film grafted to the silicon surface through epoxysilane monolayer is shown in Fig. 1a. The SEBS film was uniform without islands, holes, and areas of dewetting. The topographical image revealed light surface waviness on a generally smooth film surface. The film surface microroughness, within a 1 μm x 1 μm, area, was 0.2– 0.3 nm. The phase image (Fig. 1b) clearly shows the microphase separation typical for the ABA triblock copolymers with immiscible blocks [22-25]. Small circular and cylindrical domains with a diameter of 8-12 nm were regularly dispersed in the matrix. Thus, the film possessed the microdomain structure typical for thermoplastic elastomers, in which the PS phase forms the network crosslinking the

elastomeric matrix. Grafted SEBS film morphology is described in detail elsewhere [20, 21].

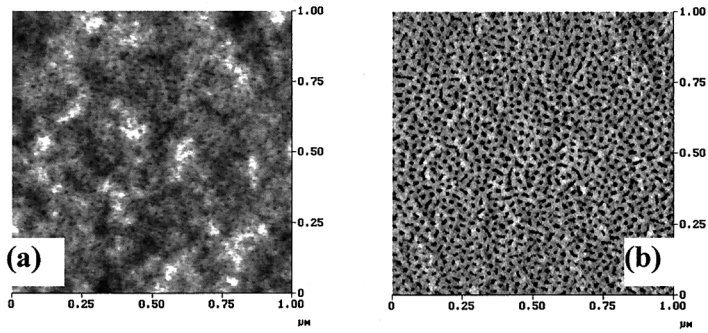

Fig. 1. SPM topographical (a) and phase (b) images of SEBS film with the thickness 8.5 nm. Vertical scale is 7.0 nm and 20 degree for topographical and phase image, respectively. Bright parts correspond to higher features and phase shifts.

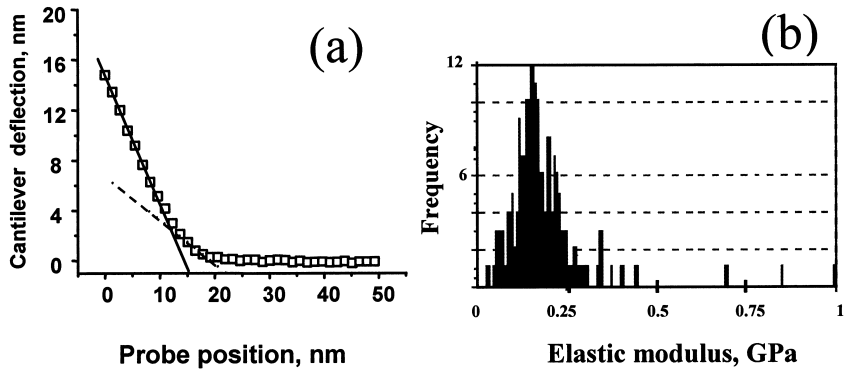

Fig. 2. (a) typical force distance curve (approach) recorded for SEBS film. (b) elastic modulus distribution within 1μm x 1μm area for SEBS film grafted to silicon substrate. Loading rate 20 nm/sec. Dashed and solid lines indicate initial and final FDC slope, respectively.

Micromechanical properties of the grafted SEBS film were tested by SPM. The objective was to prove that the elastomeric film with the thickness of 8.5 nm behaves as a rubbery compliant layer. Thus, this layer could reduce the stresses and deformations developing in the thin polymer film deposited on the inorganic surface. We recorded force-distance curves (FDC) in force-volume mode to obtain the elastic modulus of the

SEBS film. A typical FDC for the SEBS film is presented in Fig. 2a. The SPM tip advanced toward the surface and then indented into the SEBS film. At initial penetration, the slope of FDC was relatively low and indicated the presence of a compliant layer on the silicon surface. When the tip advanced further, it squeezed the rubbery layer and the value of the slope became close to the one obtained for a bare silicon substrate.

The data was analyzed within JKR theory according to the approach described in Refs. 26, 27. Analysis of tip indentation for variable loads at initial stages (less than 4 nm indentation depth and loading rate of 20nm/sec) produced an effective elastic modulus between 100 - 200 MPa for the SEBS film deposited on the surface of the silicon wafer. Surface distribution of elastic properties was fairly homogeneous (Fig. 2b). Nanoprobing of the tethered elastomeric layer at various probe velocities clearly showed the rate dependence of the measured elastic modulus due to the viscoelastic phenomenon [28]. Thus, the SEBS layer behaved in many aspects as a rubber and could, therefore, serve as a compliant interlayer in thin polymer films.

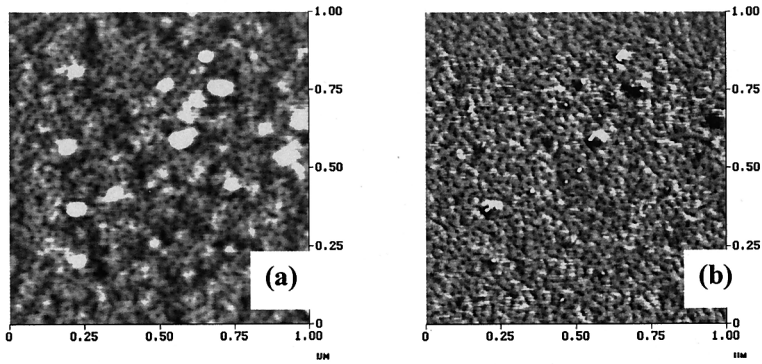

Fig. 3. SPM topographical (a) and phase (b) images of SEBS film after the spincoated EP/PPP mixture was washed out. Vertical scale is 7.0 nm and 20 degree for topography and phase images, respectively. Bright parts correspond to higher features and phase shifts.

We built bilayered coating by deposition of the EP/PPP layer on top of the grafted SEBS layer. It was checked if the SEBS layer could be washed out after the spincoating of the upper layer. Fig. 3 shows the morphology of SEBS layer after the uncured EP/PPP film was removed by rinsing with THF. Both topography and phase images show that the elastic SEBS layer remains unchanged after spincoating. We

again observed the phase separated structure typical for the grafted SEBS layer (Compare Fig. 1 a, b and Fig. 3).

Different concentrations (0.15% - 0.7%) of EP/PPP solution were used to produce top layers with thicknesses from 4 nm to 22 nm. For some EP/PPP films spincoated from the concentrated solutions, a small fraction of aggregates was observed on the surface. We believe that the aggregates formed in the solution by the reaction between EP and PPP and then were deposited on the surface. Generally, the films were complete on a microscopic level, except the thinnest one (image not shown). The thinnest film produced from the 0.15% solution (ellipsometry thickness 4 nm) did not form a uniform layer. We found droplets of the EP/PPP mixture randomly distributed on the top of the SEBS layer. Conversely, the EP/PPP mixture deposited from the 0.15% solution on the bare silicon wafer gave a continuous film.

The instability of the thinnest film on top of the SEBS layer during the spincoating could be connected with the low surface energy of the SEBS layer (water contact angle 100° for SEBS against 5° for the silicon wafer). For the films produced from 0.3 – 0.5 % solution (ellipsometry thickness 9, 13 and 16 nm), we observed the formation of small holes (images not shown). The hole formation indicates that the very first stage of dewetting occurred during the deposition of the EP/PPP mixture on the low energy surface of SEBS layer [5]. The amount of the holes decreases when the thickness of the EP/PPP layer reached 19 nm. Only several tiny holes per scanned area (10x10 μm) were observed for the films produced from 0.6 – 0.7 % solution (thickness 19 - 22 nm) (images not shown).

To reach optimal properties, bulk EP/PPP mixture was cured at the temperature well above 100 °C for 5-10 hours (see experimental part). The same regime was used for the solidification of the thin film. Initially homogeneous, the film completely dewetted the SEBS surface when heated above 100 °C. There are two concurrent processes during the top layer solidification at high temperature: crosslinking and decrease of viscosity. The crosslinking reaction should prevent the dewetting. However, the rate of dewetting is inversely proportional to the viscosity [7]. Decrease of the viscosity provokes the dewetting processes before the film could be stabilized by the network formation.

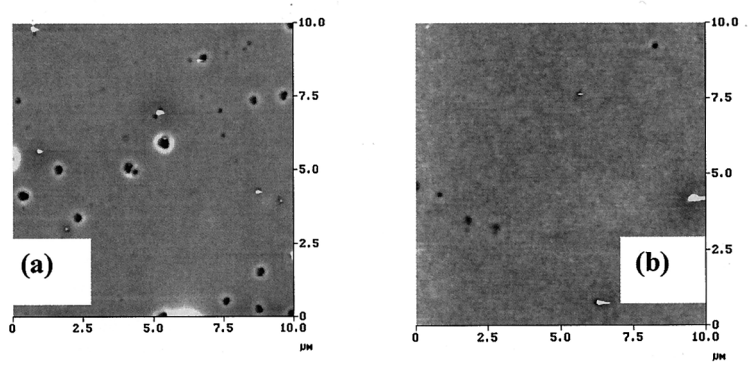

Fig. 4. SPM topographical images of EP/PPP composite films with a thickness of 16 nm (a) and 19 nm (b) after curing. Vertical scale is 50 nm (a) and 20 nm (b) Bright parts correspond to higher features.

Consequently, in the next experiment, curing of the EP/PPP composite layer was initiated at 45 °C for 15 hours. The films were annealed at 55 °C, 75 °C, and 90 °C for 15 hours. The solidification was completed at 110 °C (15 hours). We chose this procedure to initiate the crosslinking before the viscosity of EP/PPP mixture became too low and dewetting occurred. After each annealing step, the morphology of the films was examined by SPM. The results indicated that the morphology remained almost unchanged during annealing due to chemical crosslinking (Fig. 4).

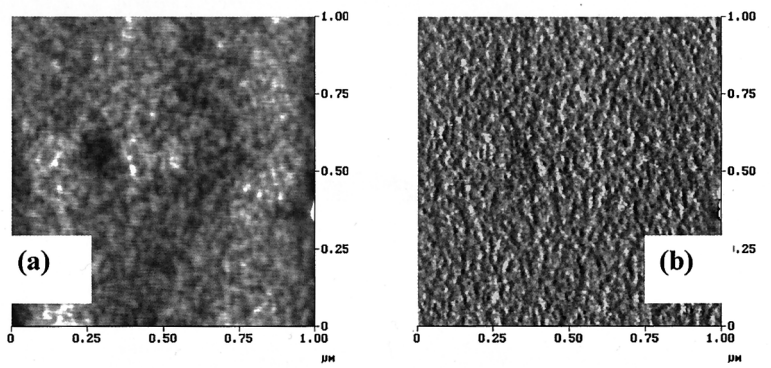

Fig. 5. SPM topographical (a) and phase (b) images of EP/PPP layer (21 nm) after the solidification. Vertical scale is 15 nm and 20 degree for topography and phase images, respectively. Bright parts correspond to higher features and phase shifts.

Fig. 5 shows the higher magnification SPM topographical and phase images of EP/PPP film (thickness 21 nm) deposited on top of the SEBS film. Similar morphology was observed for the films with different thicknesses. The EP/PPP layers were smooth and uniform on the microscopic level (Fig. 5a). The SPM microroughness of the films within 1 μm x 1 μm area was 0.35 nm. Phase imaging showed that the surface areas with slightly variable adhesion were randomly distributed (Fig. 5b). Consequently, there was no phase segregation of EP and PPP during the curing. Thus, EP/PPP material, forming the topmost layer of the bilayered film, was homogeneous on the microscopic level.

Selected annealed films were washed by multiple rinsing with THF and DMSO including the washing in an ultrasonic bath. The surface morphology of the film after the washing is presented in Fig. 6. The film morphology showed little change as a result of the washing. Moreover, the ellipsometry measured thickness of the film was the same before and after the solvent treatment. The obtained results showed that the curing of the film was complete and the EP/PPP layer was strongly attached to the SEBS layer.

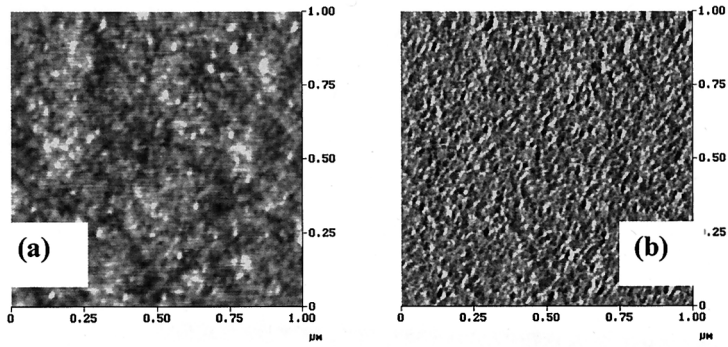

Fig. 6. SPM topographical (a) and phase (b) images of cured EP/PPP layer (21 nm) after the washing with THF and DMSO. Vertical scale is 8 nm and 7 degree for topography and phase images, respectively. Bright parts correspond to higher features and phase shifts.

It was important to prove that the EP/PPP mixture did not penetrate inside the SEBS layer at elevated temperatures and that the segregated bilayered structure was, indeed, obtained. To show this, we cured the incomplete EP/PPP film obtained by spincoating from the 0.15% solution.

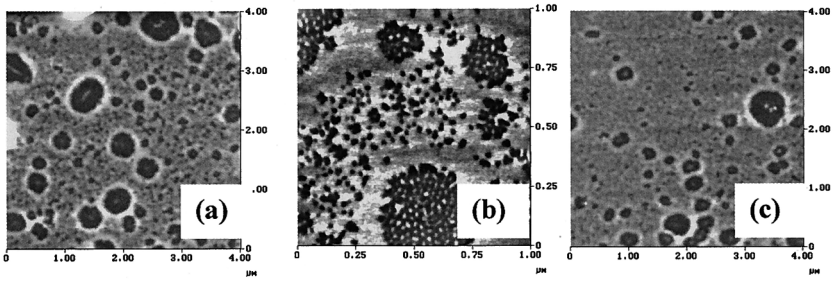

Fig. 7. SPM topographical ((a) and (c)) and phase (b) images of EP/PPP films produced from 0.15 % solution. Annealed at 55 °C ((a) and (b)) and 110 °C (c). Vertical scale is 60 nm and 20 degree for topography and phase images, respectively. Bright parts correspond to higher features and phase shifts.

When the sample was annealed at 45 °C – 55 °C (15 hours), the droplets formed during the spincoating partially spread on the surface and the dewetted morphology shown in Fig. 7a was formed. The phase separated structure typical for the grafted SEBS layer was clearly observed underneath of the incomplete film (Fig. 7b). Then, the film was annealed at 75 °C and 90 °C for 15 hours. The curing was completed at 110 °C (15 hours). Fig. 7c shows the structure of the film after the curing. The film morphology did not change in the course of the solidification. We measured the thickness of the EP/PPP layer annealed at different temperatures by SPM. No change was observed in the thickness during the curing of the EP/PPP layer. The results unambiguously showed that the EP/PPP layer did not penetrate inside the elastic primary layer during the solidification at the elevated temperatures. Thus, we fabricated the truly layered film ((EP/PPP)/SEBS/Si) consisting of the primary elastic and top hard layers.

Micromechanical properties of the bilayered composite film

Force-distance curves were recorded for (EP/PPP)/SEBS/Si to determine if the compliant rubbery layer underneath the high modulus layer influenced the mechanical properties of the bilayered coatings. For the sake of comparison, measurements were also taken for the EP/PPP films deposited on the bare silicon ((EP/PPP)/Si) cured under the same conditions as (EP/PPP)/SEBS/Si.

The slope of the force-distance curve was determined at the same tip deflection (3 nm) or identical applied force. Lower slope corresponds to a more compliant film. The values of the FDC slope versus the thickness of the EP/PPP layer are shown in Fig. 8. The data points presented in the Fig. 8 were averaged over 12-20 measurements from different surface locations.

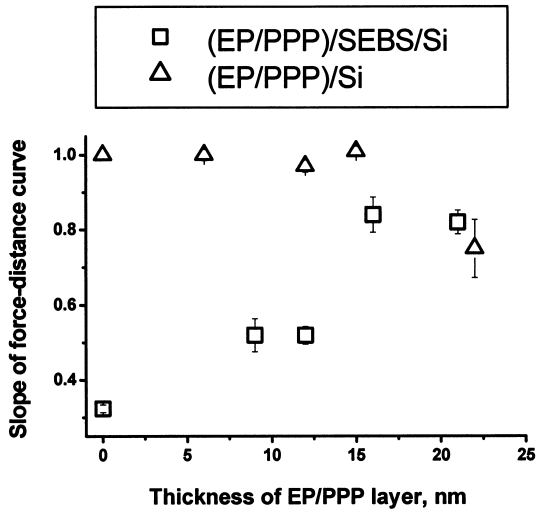

Fig. 8. The slope of force-distance curve for (EP/PPP)/SEBS/Si and (EP/PPP)/Si versus the thickness of EP/PPP layer. 1.0 corresponds absolutely stiff surface.

As can be concluded from these data, when the thickness of the film is about 20 nm, the FDC slope is similar for both (EP/PPP)/SEBS/Si and (EP/PPP)/Si. The slope observed for the films is lower than the one detected for bare silicon wafer. Hence, the SPM tip indented into the layer and caused the elastic surface deformation before the stress was transferred to the silicon substrate. However, there was no noticeable influence of SEBS elastomeric interlayer on the micromechanical behavior of the film with the thickness >16 nm. When the thickness decreased, pronounced differences in the mechanical behavior between (EP/PPP)/Si and (EP/PPP)/SEBS/Si was observed. The FDC slope for (EP/PPP)/Si increased and became close to the one obtained for the bare silicon wafer. Thus, the (EP/PPP)/Si layer was not detected by SPM force-distance measurements. The stress applied to the film was transferred through the ultrathin EP/PPP layer to the silicon substrate. On the other hand, the slope for

(EP/PPP)/SEBS/Si decreased. The underlying SEBS layer clearly affected the mechanical properties of the bilayered film. The bilayered (EP/PPP)/SEBS/Si film sustained much higher elastic deformations in comparison with the (EP/PPP)/Si film of analogous thickness. Thus, the rubbery SEBS layer absorbed part of the applied stress and served as a compliant interlayer capable of reducing the stress originating from dissimilarity in physical properties between the polymer coating and the inorganic substrate.

Conclusions

We fabricated bilayered nanocomposite coatings with total thickness less than 30 nm consisting of a hard polymer layer placed on top of an elastomeric layer. The primary SEBS layer was attached to the surface by melt grafting to a chemically reactive silicon surface functionalized with an epoxy-terminated SAM. The SEBS layer behaved as a rubbery material that could serve as a compliant interlayer in thin polymer film. We synthesized the bilayered film by the deposition of the EP/PPP layer on top of the grafted SEBS layer by spincoating. The solidification of the topmost layer was initiated at low temperatures (40 – 50 ^{0}C) to avoid dewetting. The curing of the film was finished at 110 ^{0}C (15 hours). The EP/PPP layer was strongly attached to SEBS layer. It was found that the EP/PPP layer did not penetrate into the elastic primary layer during the solidification process.

The elastic response of the hard polymer layer on a normal external load was affected by the underlying elastomeric layer. Indeed, the SEBS layer served as a compliant interlayer capable of damping interfacial stresses originated from dissimilarity in the physical properties between the polymer coating and inorganic substrate. The influence of the bilayered structure on the ultimate microtribological properties of bilayered nanocomposite coatings is a focus of further investigation.

Acknowledgements

This work is supported by The US National Science Foundation, CMS-9996445 Grant. The authors thank Dr. S. A. Chizhik and Dr. V. V. Gorbunov for helpful discussion.

We are grateful to Dr. V. Gorbunov for help with the FDC analysis and elastic modulus calculation. The authors also thank Shell Chemical Co. for donating SEBS sample.

References

1. Z. W. Wicks, F. N. Jones, S. P. Pappas, *Organic Coating: Science and Technology*, Wiley-Interscience, New York 1992
2. P. Müller-Buschbaum, M. Stamm, *Macromolecules* **31**, 3668 (1998)
3. D. Raghavan, X. Gu, T. Nguyen, M. VanLandingham, A. Karim, *Macromolecules* **33**, 2573 (2000)
4. R. Limary, P. F. Green, *Langmuir* **15**, 5671 (1999)
5. G. Reiter, *Phys. Rev. Lett.* **68**, 75 (1992)
6. R. Xie, A. Karim, J. F. Douglas, C. C. Han, R. A. Weiss, *Phys. Rev. Lett.* **81**, 1251 (1998)
7. I. W. Hamley, E. L. Hiscutt, Y.–W. Yang, C. Booth, *J. Colloid Interface Sci.* **209**, 255 (1999)
8. Cambridge Engineering Selector 3.0. Granta Design Limited, 1999.
9. C. Coupeau, J. F. Naud, F. Cleymand, P. Goudeau, J. Grilhé, *Thin Solid Films* **352**, 194 (1999)
10. J. Bouchet, A. A. Roche, P. Hamelin, *Thin Solid Films* **355-356**, 270 (1999)
11. R. Yerushalmi-Rozen, J. Klein, L. J. Fetters, *Science* **263**, 793 (1994) A. Karim, V. V. Tsukruk, J. F. Douglas, S. K. Satija, L. J. Fetters, D. H. Reneker, M. D. Foster, *J. Phys. II France* **1995**, *5*, 1441.
12. V.V. Tsukruk, I. Luzinov, D. Julthongpiput, *Langmuir* **15**, 3029 (1999).
13. I. Luzinov, D. Julthongpiput, A. Liebmann-Vinson, T. Cregger, M. D. Foster, V. V. Tsukruk, *Langmuir* **16**, 504 (2000)
14. G. Henn, D. G. Bucknall, M. Stamm, P. Vanhoorne, R. Jerome, *Macromolecules* **29**, 4305 (1996)
15. C. A. May, Ed. *Epoxy Resins: Chemistry and Technology* M. Dekker, New York, 1988
16. A. J. Pasquale, V. V. Sheares, *Polym. Prepr. (Am. Chem. Soc. Div. Polym. Chem.)* **39(1)**, 331 (1998)
17. D. W. Van Krevelen, *Properties of Polymers* Elsevier, Amsterdam 1997

18. V. V. Tsukruk, *Rubber Chem. Techn.* **70(3),** 430 (1997). V. V. Tsukruk, D. H. Reneker, *Polymer* **36**, 1791 (1995)

19. B. Ratner, V. V. Tsukruk, Eds. *Scanning Probe Microscopy of Polymers, ACS Symposium Series* 1998, *v. 694*

20. I. Luzinov, D. Julthongpiput, V. V. Tsukruk, *Macromolecules*, **33,** 7629 (2000)

21. I. Luzinov, D. Julthongpiput, V. V. Tsukruk, *Polymer*, ***42,*** *2267,* (2000)

22. S. N. Magonov, J. Cleveland, V. Elings, D. Denley, M.-H. Whangbo, *Surface Science* **389**, 201 (1997)

23. M. A. Van Dijk, R. van den Berg, *Macromolecules* **28**, 6773 (1995)

24. G. Kim, M. Libera, *Macromolecules* **31,** 2569 (1998)

25. M. Motomatsu, W. Mizutani, H. Tokumoto, *Polymer* **38**, 1779 (1997)

26. S. A. Chizhik, Z. Huang, V. V. Gorbunov, N. K. Myshkin, V. V. Tsukruk, *Langmuir* **14,** 2606 (1998)

27. V. V. Tsukruk, Z. Huang, *Polymer* **41**, 5541 (2000)

28. Sperling, L. H. *Introduction to Physical Polymer Science,* John Wiley & Sons, Inc., 1992.